An Advanced Computer Algorithm for Determining Morphology Development in Latex Particles

YVON G. DURANT and DONALD C. SUNDBERG*

Polymer Research Group, University of New Hampshire, Durham, New Hampshire 03820

SYNOPSIS

A new algorithm is presented for the prediction of equilibrium morphology in latex particles. Thermodynamic equilibrium calculations of the interfacial free energies associated with a large array of possible morphologies serve to create a continuous free-energy surface upon which the preferred morphology is located. When the computations are performed on a 486DX33 PC, the calculations are essentially instantaneous. The graphical output can be refreshed on the monitor screen in less than 2 s. The algorithm is applied to simulate the conversion-dependent morphology for several latex systems composed of polystyrene and poly(methyl methacrylate) and two very different surfactants. © 1995 John Wiley & Sons, Inc.

INTRODUCTION

The morphology of multistage emulsion particles has become an increasingly important subject during the last decade. A wide variety of structures, such as those represented in Figure 1, have been reported as a result of a variety of experimental investigations.[1-5] Equilibrium morphologies are achieved when the rate of diffusion of a chain is much faster than is the polymerization rate. Kinetic-controlled morphologies are obtained when phase separation proceeds more slowly than the polymerization rate. At this point in time, the modeling of composite latex particle morphology has reached a significant level of sophistication. The early models for two-component particles based upon thermodynamic equilibrium considerations applicable only at the end of the latex production process[6-10] have been expanded to include conversion-dependent pathways[11-14] and three-component particles.[15] Although all present models are restricted to thermodynamic equilibrium conditions (i.e., phase-separation kinetics being much faster than polymerization kinetics), a significantly wide variety of particle morphologies have been considered,[16] including moon-like structures,[11,14] occluded structures,[11,12] and sandwich structures.[12] Three-component particles are dramatically richer in thermodynamically stable morphological complexities, but can also be modeled in a straightforward manner.[15] The purpose of the present work was to offer a new computational approach which leads to the generation of a graphic display of the free-energy surface for a continuous spectrum of different equilibrium morphologies and from which the user can readily follow the conversion-dependent morphology pathway. The computation of the energy surface is essentially instantaneous on a 486DX33 PC. Phase diagrams and particle morphologies are displayed on the same screen, which can be refreshed in less than 2 s. The graphical presentation is enhanced by using a color output to highlight the various free-energy levels in the continuous surface-energy spectrum.

THERMODYNAMIC CONSIDERATIONS

The concept of predicting two-component particle shapes via the minimization of the interfacial energy was first applied by Torza and Mason[17] in their study of immiscible oil droplets suspended in water. Later, Sundberg and co-workers[6] extended this work with applications to polymer particles by the use of eq. (1):

$$\Delta\gamma = \Delta G/A_0 = \sum_i (A_i/A_0)\gamma_i \qquad (1)$$

* To whom correspondence should be addressed.

Journal of Applied Polymer Science, Vol. 58, 1607–1618 (1995)
 CCC 0021-8995/95/091607-12

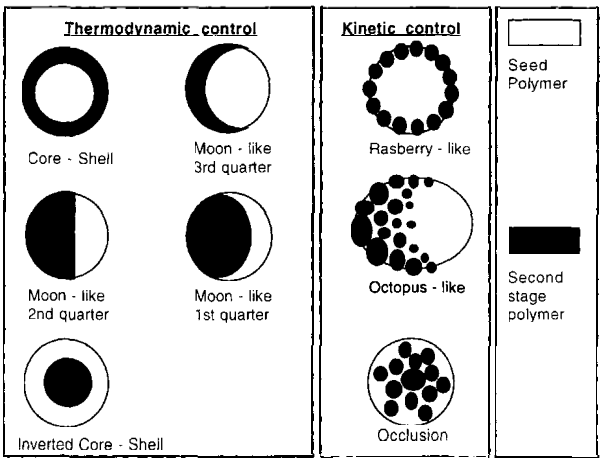

Figure 1 Some examples of morphologies of two-phase latex particles.

where $\Delta\gamma$ is the reduced free energy; A_i, the surface area of interface i; A_0, the initial surface area of the seed latex particle; and γ_i, the interfacial tension. The present work describes a conversion-dependent version of eq. (1) with a continuous spectrum of morphologies considered. Here, the seed polymer is denoted as P_1, the second-stage monomer as M, and the second-stage polymer as P_2. The two polymers are considered to be totally immiscible with each other and insoluble in the aqueous phase. The monomer is distributed between the two polymer phases and the aqueous phase, and its concentration in each phase is computed via its chemical potentials, as shown below. The calculations of the various monomer concentrations are very important as they influence the interfacial tensions at all the polymer interfaces. Furthermore, the polymer/monomer interaction parameters, $\chi_{M/P}$, are also dependent on monomer concentration. The calculations are done in three steps, the first being the partitioning of the monomer between the two polymer phases and the aqueous phase. Then, the volumes of the two polymer phases are computed at the chosen conversion level. Finally, a particle morphology is assumed and its reduced free energy is calculated. This sequence of computations is shown in the flow chart of Figure 2. Obviously, some parameters must be known prior to the calculation process; among these are the polymer molecular weights, densities of all components, and the saturation concentration of monomer in the aqueous phase.

Partitioning of the Monomer Between the Phases

At an arbitrary point of conversion during the reaction, any of the morphologies depicted in Figure 1 consists of two polymer phases (both containing monomer) surrounded by an aqueous phase. Under equilibrium conditions, one can write that the chemical potential of the monomer is the same in all three phases:

$$\mu_M^A = \mu_M^{P1} = \mu_M^{P2} \tag{2}$$

where A designates the aqueous phase. Expressions for each of these chemical potentials can be written in traditional form as

$$\mu_M^A = \mu_M^0 + RT \operatorname{Ln} \frac{X_M}{X_M^S} \tag{3}$$

$$\mu_M^{P1} = \mu_M^0 + RT[\operatorname{Ln} \Phi_M^{P1} + (1 - \Phi_M^{P1})(1 - m_1) + \chi_{M/P1}(1 - \Phi_M^{P1})^2] \tag{4}$$

$$\mu_M^{P2} = \mu_M^0 + RT[\operatorname{Ln} \Phi_M^{P2} + (1 - \Phi_M^{P2})(1 - m_2) + \chi_{M/P2}(1 - \Phi_M^{P2})^2] \tag{5}$$

where μ_M^0 is the chemical potential of the pure monomer; X_M^S, the monomer solubility in water; Φ_M^{Pk}, the volume fraction of monomer in phase k; $\chi_{M/Pk}$, the Flory–Huggins monomer/polymer k interaction parameter; $m_k = V_M/V_{Pk}$; V_M, V_{Pk}, the molar volumes of the monomer and the polymer k, respectively, and X_M, mol fraction of monomer in the aqueous phase. We omitted the Morton term describing the influence of the latex particle surface, since it is far too small to influence the calculations

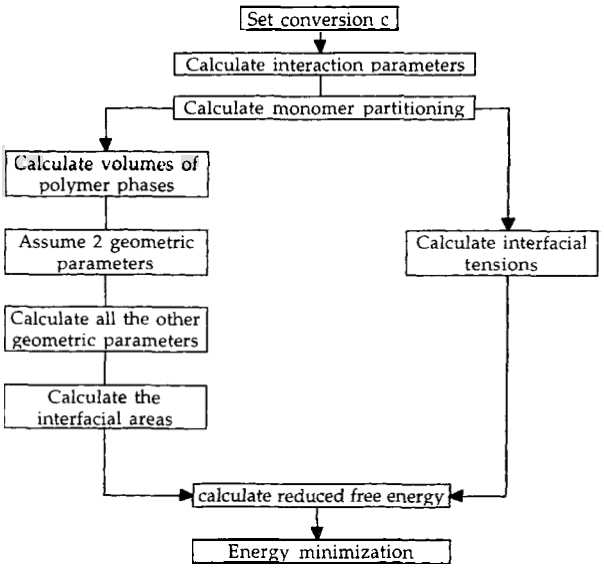

Figure 2 Flow chart for the calculation of the reduced free energy of a two-phase latex particle at a given monomer conversion.

at all conditions other than maximum particle swelling.[18-20]

At a given conversion, the amount of monomer converted into polymer is known, so one can write a material balance on the monomer:

$$n_M^0 = n_M^A + n_M^{P1} + n_M^{P2} + n_{P2} \tag{6}$$

where n_M^k ($k = 0, A, P1, P2$) are the moles of monomer at zero conversion ($k = 0$), in the aqueous phase, and in phases 1 and 2, respectively, and n_{P2} is the number of moles of monomer converted in polymer 2. Solving eq. (6) for n_M^{P2} and using the definition of conversion as $c = n_{P2}/n_M^0$ yields

$$n_M^{P2} = n_M^0(1 - c) - n_M^A - n_M^{P1} \tag{7}$$

Relating the moles of monomer in each polymer phase to the related volume fraction of monomer, Φ_M^{Pk}, results in

$$\Phi_M^{P1} = \frac{1}{\left(1 + \frac{n_{P1}}{n_M^{P1}} \frac{Mw_{P1}}{Mw_M} \frac{d_M}{d_{P1}}\right)} \tag{8}$$

$$\Phi_M^{P2} = \frac{1}{\left(1 + \frac{n_{P2}}{n_M^{P2}} \frac{d_M}{d_{P2}}\right)} \tag{9}$$

where Mw_k is molecular weight and d_k is density for each component k. The mol fraction of monomer in the aqueous phase is given by

$$X_M = \frac{1}{\left(1 + \frac{M_{\text{aqueous}}}{18 n_M^A}\right)} \tag{10}$$

where M_{aqueous} is the total mass of the aqueous phase and the factor 18 represents the molecular weight of water.

Taking the chemical potential of pure monomer in its reference state to be zero, eqs. (4) and (5) can individually be equated to eq. (3). Then, in combination with eq. (7), we have a system of three equations and three unknowns n_M^k ($k = A, P1, P2$) as shown below:

$$\text{Ln}\frac{X_M}{X_M^S} = \text{Ln}\,\Phi_M^{P1} + (1 - \Phi_M^{P1})(1 - m_1) + \chi_{M/P1}(1 - \Phi_M^{P1})^2 \tag{11}$$

$$\text{Ln}\frac{X_M}{X_M^S} = \text{Ln}\,\Phi_M^{P2} + (1 - \Phi_M^{P2})(1 - m_2) + \chi_{M/P2}(1 - \Phi_M^{P2})^2 \tag{12}$$

$$n_M^{P2} = n_M^0(1 - c) - n_M^A - n_M^{P1} \tag{13}$$

The method used to solve these equations is given in Table I. It is to be noted that the interaction parameter can be a function of Φ_M^{Pk} and that an elastic term (crosslinked systems) could be added to the expressions for the chemical potentials, with no modification of the above calculation scheme.

When the calculation of the monomer partitioning is finished, the volume of the two polymer phases can be calculated as

$$V_{P1} = \left(\frac{n_M^{P1} \cdot Mw_M}{d_M} + \frac{n_{P1} \cdot Mw_{P1}}{d_{P1}}\right)\frac{1}{N_P} \tag{14}$$

$$V_{P2} = \left(\frac{n_M^{P2}}{d_M} + \frac{n_{P2}}{d_{P2}}\right)\frac{Mw_M}{N_P} \tag{15}$$

where N_p is the number of seed latex particles, and Nw_{P1}, the molecular weight of the monomer used to make polymer 1. All these computations are done without regard to the latex particle morphology and comprise one module within the overall algorithm used to calculate free energies. This is shown in Figure 2 and discussed in the next section.

GEOMETRIC CONSIDERATIONS

The general geometry of the two-phase particle considered in this work is the same as that reported earlier,[14] but a new set of variables is used to reduce the complexity of the equations of the earlier anal-

Table I Computational Method for Monomer Partitioning

Assume a value of n_M^{P1} in the range $[0, n_M^0]$
Calculate Φ_M^{P1} using eq. (8)
Calculate $Y_1 = \text{Ln}\,\Phi_M^{P1} + (1 - \Phi_M^{P1})(1 - m_1) + \chi_{M/P1}(1 - \Phi_M^{P1})^2$
Calculate $X_M = X_M^S \exp(Y_1)$
Calculate n_M^A from eq. (10)
Calculate n_M^{P2} from eq. (13)
Calculate Φ_M^{P2} from eq. (9)
Calculate $Y_2 = \text{Ln}\,\Phi_M^{P2} + (1 - \Phi_M^{P2})(1 - m_2) + \chi_{M/P2}(1 - \Phi_M^{P2})^2$
A new value of n_M^{P1} is assumed to get convergence of $(Y_1 - Y_2)$ toward 0.

ysis. Figure 3 shows a cross section of the general morphology with all the geometric angles and radii displayed.

Various combinations of these variables will yield a continuous array of morphologies on a planar surface with four principle axes (α_1, β_1 and α_2, β_2) as shown in Figure 4. In Figure 5 are displayed some of the fully phase-separated morphologies with the seed polymer in black and the second stage polymer in gray. In Figures 4 and 5, three domains are distinguished: On the left, in light gray, the first domain has a convex seed polymer phase. The second domain, in the center, in white, has a flat polymer/polymer interface. On the right, in dark gray, the third domain has a concave seed polymer phase. At the $\alpha_1 = \pi$ location, the morphology is described as core–shell (CS); at $\alpha_2 = \pi$, as inverted core–shell (ICS); and at $\alpha_1 = \alpha_2 = 0$, as individual particles (IP). All the other locations display intermediate morphologies, some of which are commonly described as hemispheres and moonlike or engulfed structures.

The monomer partitioning thermodynamics allows one to compute the volumes of the two polymer/monomer phases at any extent of conversion during the reaction. To compute the reduced free energy of the composite particle [eq. (16)], the surface areas of the interfaces must be computed:

$$\Delta\gamma = \Delta G/A_0 = \frac{A_1\gamma_{P1/W} + A_2\gamma_{P2/W} + A_i\gamma_{P1/P2} - A_0\gamma_{P1/W}}{A_0} \quad (16)$$

where A_1 represents the area of the aqueous/polymer 1 interface; A_2, that for polymer 2; A_0, that of the seed latex particle; and A_i, the organic interface

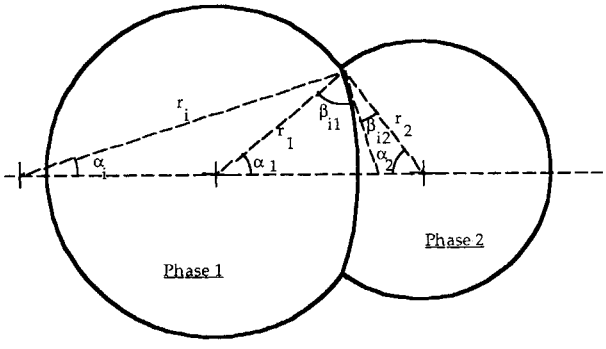

Figure 3 Cross section of the general geometry studied in this model. All interfaces are portions of spheres and phase 1 contains the seed polymer.

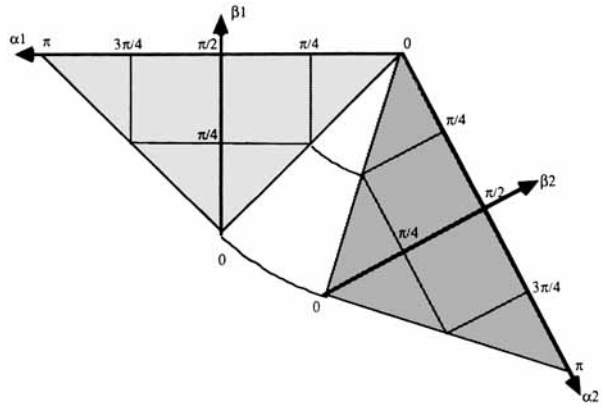

Figure 4 Continuous array of morphologies on a planar surface having four principal axes.

between polymer 1 and polymer 2, and W designates water (including the presence of surfactants, initiator end groups, etc., if any), and γ_{kl}, the interfacial tension between phases k and l. The surface-area calculations are somewhat complicated and it is helpful to divide the morphology map displayed in Figure 4 into three distinct domains: The first one takes the seed polymer phase 1 as convex, the second has a flat polymer/polymer interface, and the third has phase 1 as concave.

Phase 1 Convex

Consideration of the problem shows that beside the conversion c one needs to assume the values of two additional variables. It is obvious that the geometric model contains eight variables (r_1, r_2, r_i, α_1, α_2, α_i, β_1, β_2) in addition to the conversion c. We write four geometric and two volumetric relationships [eqs. (18) and (21)]. The new approach suggests that one assumes values for α_1 and β_1 at the start. It is clear

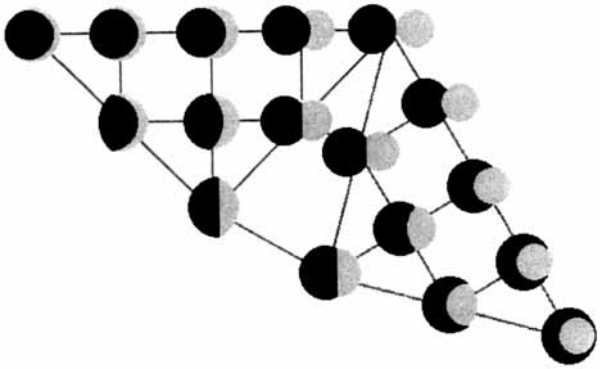

Figure 5 Illustrative topological map corresponding to Figure 4.

that α_1 must be in the range $[0, \pi]$. As we have restricted the shape of phase 1 to be convex, one limit on β_1 is a flat interface; the other is a spherical interface of same radius as sphere 1. In quantitative terms, these limits appear as

$$\text{Flat interface} \quad 0 \le \alpha_1 \le \frac{\pi}{2}, \quad \beta_1 = \frac{\pi}{2} - \alpha_1$$

$$\text{Spherical interface} \quad \frac{\pi}{2} \le \alpha_1 \le \pi, \quad \beta_1 = \alpha_1 - \frac{\pi}{2}$$

$$\text{Engulfment} \quad 0 \le \alpha_1 \le \pi, \quad \beta_1 = 0$$

Between the three limits shown above, one chooses a value of α_1 and a value of β_1. α_i is easily calculated with the relation

$$\alpha_i = \alpha_1 + \beta_1 - \frac{\pi}{2} \tag{17}$$

and then the volume of phase one is written as

$$V_{P1} = \frac{\pi}{3}\{r_1^3[4 - (1 - \cos\alpha_1) \times (2 - (\cos\alpha_1)^2 - \cos\alpha_1)] + r_i^3(1 - \cos\alpha_i)(2 - (\cos\alpha_i)^2 - \cos\alpha_i)\} \tag{18}$$

A simple geometric relationship also exists between the three spheres and can be expressed as

$$r_i \cdot \sin\alpha_i = r_1 \cdot \sin\alpha_1 = r_2 \cdot \sin\alpha_2 \tag{19}$$

By combining eqs. (18) and (19), it is possible to calculate r_1 as

$$r_1 = \left\{\frac{3V_{P1}}{\pi\left\{[4 - (1 - \cos\alpha_1)(2 - (\cos\alpha_1)^2 - \cos\alpha_1)] + \left(\frac{\sin\alpha_1}{\sin\alpha_i}\right)^3(1 - \cos\alpha_i)(2 - (\cos\alpha_i)^2 - \cos\alpha_i)\right\}}\right\}^{1/3} \tag{20}$$

Turning to phase 2, its volume can be written as

$$V_{P2} = \frac{\pi}{3}\{r_2^3[4 - (1 - \cos\alpha_2) \times (2 - (\cos\alpha_2)^2 - \cos\alpha_2)] - r_i^3(1 - \cos\alpha_i)(2 - (\cos\alpha_i)^2 - \cos\alpha_i)\} \tag{21}$$

Using eq. (19) and defining K as

$$K = \frac{3V_{P2}}{\pi(r_1 \sin\alpha_1)^3} + \frac{(1 - \cos\alpha_i)(2 - (\cos\alpha_i)^2 - \cos\alpha_i)}{(\sin\alpha_i)^3} \tag{22}$$

eq. (21) can be rearranged as follows:

$$\frac{4 - (1 - \cos\alpha_2)(2 - (\cos\alpha_2)^2 - \cos\alpha_2)}{(\sin\alpha_2)^3} - K = 0 \tag{23}$$

Since at any condition of interest, V_{P2} is known from eq. (15) and α_i and r_1 are calculated from eqs. (17) and (20), respectively, eqs. (22) and (23) can be solved for α_2 ($0 \le \alpha_2 \le \pi$).

With all the geometric angles and radii known, the interfacial areas can be calculated as

$$\begin{cases} A_1 = 2\pi r_1^2(1 + \cos\alpha_1) \\ A_2 = 2\pi r_2^2(1 + \cos\alpha_2) \\ A_i = 2\pi r_i^2(1 + \cos\alpha_i) \end{cases} \tag{24}$$

These areas can now be used to compute the reduced free energy via eq. (16).

Flat Interface

For the case of a flat interface between phases 1 and 2 shown in Figure 3, the calculations are simpler as they present a limit of the previous calculations. A value of α_1 is chosen within the limit $0 \le \alpha_1 \le \frac{\pi}{2}$.

The volume of phase 1 can be expressed as

$$V_{P1} = \frac{\pi}{3} r_1^3[4 - (1 - \cos\alpha_1) \times (2 - (\cos\alpha_1)^2 - \cos\alpha_1)] \tag{25}$$

from which r_1 can be determined. Further,

$$A_i = \pi r_1^2[1 - (\cos\alpha_1)^2] \tag{26}$$

$$A_1 = 2\pi r_1^2[1 + (\cos\alpha_1)^2] \tag{27}$$

r_2 and α_2 are connected through the geometric relation (28) and the volume equation (29):

$$r_1 \sin \alpha_1 = r_2 \sin \alpha_2 \quad (28)$$

$$V_{P2} = \frac{\pi}{3} r_2^3[4 - (1 - \cos \alpha_2) \times (2 - (\cos \alpha_2)^2 - \cos \alpha_2)] \quad (29)$$

A combination of (28) and (29) can be used to solve for α_2 first, then r_2.

Finally, we can calculate A_2:

$$A_2 = 2\pi r_2^2[1 + (\cos \alpha_2)^2] \quad (30)$$

As before, the interfacial areas from eqs. (26), (27), and (30) can be used to calculate the reduced surface energy from eq. (16).

Phase 1 Concave

When phase 1 is concave, phase 2 is convex. Thus, the appropriate calculations can be made by switching the subscripts "1" and "2" in eqs. (17)–(24).

A computer program has been written in Pascal on a 486DX33 PC. The output needs three dimensions to be displayed (two geometric parameters and the resulting reduced free energy). At a given conversion, the free energy is plotted on the vertical axis and the two geometric parameters on an X/Y axis placed at a bias. The three cases evoked earlier are put together on one plot. The convex case (relative to phase 1) is placed on the left, the concave case is on the right (with a rotation of 60°), and the case of the flat polymer/polymer interface is placed between the two lines:

$$0 \leq \alpha_n \leq \frac{\pi}{2}, \quad \beta_n = \frac{\pi}{2} - \alpha_n \quad \text{with } n = 1, 2$$

Figure 5 shows the resulting morphology map representing some of the particle shapes and showing several axes.

Because of the high speed of the computer and the efficiency of the algorithm, calculations take less than 2 s for a given conversion, including the graphical display time. This high-speed computation allows the avoidance of storing procedures. The user can interact easily by setting new values of the interfacial tension or interaction parameter and get a quick answer. The main advantage of this output is the creation of a continuous surface for all the considered morphologies and one readily sees the difference between the energies of various morphologies. The minimum energy is readily found by a computer search and explicitly displayed on the surface by a circled cross. Examples of such surfaces are presented in the discussion section.

DISCUSSION

To demonstrate the output characteristics of this new computational model, we used the experimental system reported by Winzor and Sundberg.[12] Here, polystyrene (PS) or poly(methyl methacrylate) (PMMA) seed particles were swollen to 100% increased volume with methyl methacrylate (MMA) or styrene monomer and the large particle-size latices were stabilized by either sodium dodecyl sulfate (SDS) or a natural pectin (MXP). Interaction parameters were obtained from a handbook[21] or simulated via a Unifac computer program.[22] All the interfacial tensions and their variations with MMA concentration were taken from Winzor and Sundberg.

Three experimental systems were simulated in the present work and these are described in Table II. Other experimental details are contained in Winzor and Sundberg's article.[12] Figures 6 and 7 show the variations of all interfacial tensions as a function of monomer conversion for systems I, II, and III, respectively. The dependency of the interaction parameters with monomer volume fraction are shown in Figure 8.

The graphic output from the computational scheme applied to any chosen conversion level consists of a free-energy surface with the point of minimum energy denoted, a cross-sectional representation of the preferred morphology of the latex particle, and a triangular diagram on which the phase compositions are depicted at the end of the equilibrium tie line. The compositional pathway for the polymerization reaction is also displayed in the triangular diagram. Figure 9 shows these features for system III of Table II at 75% conversion of the styrene monomer. Here, the energy surface displays greatly different contours and clearly shows that an

Table II Stimulated Experiments[12]

System	Seed Polymer	Monomer	Surfactant
I	PS	MMA	MXP
II	PS	MMA	SDS
III	PMMA	Styrene	MXP

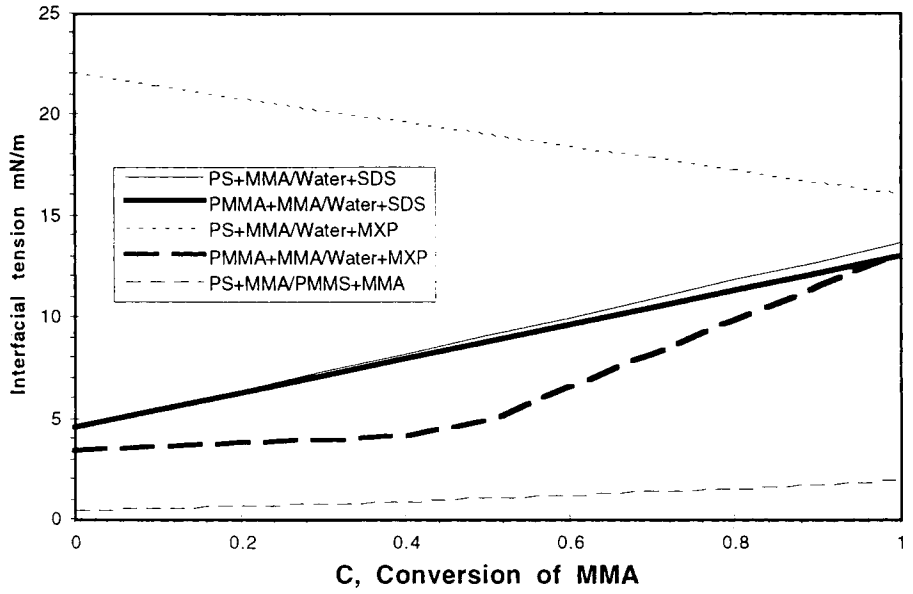

Figure 6 Interfacial tension depending on conversion between (PS + MMA)/(water + MXP), (PMMA + MMA)/(water + MXP), (PS + MMA)/(water + SDS), (PMMA + MMA)/(water + SDS), and (PS + MMA)/(PMMA + MMA), after Winzor and Sundberg.[12]

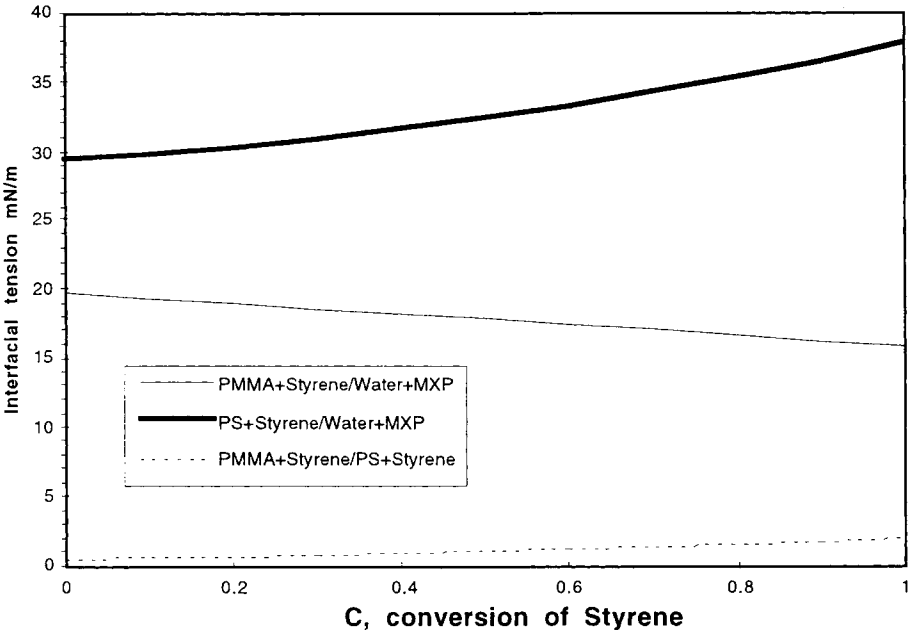

Figure 7 Interfacial tension depending on conversion between (PMMA + styrene)/(water + MXP), (PS + styrene)/(water + MXP), and (PS + styrene)/(PMMA + styrene), after Winzor and Sundberg.[12]

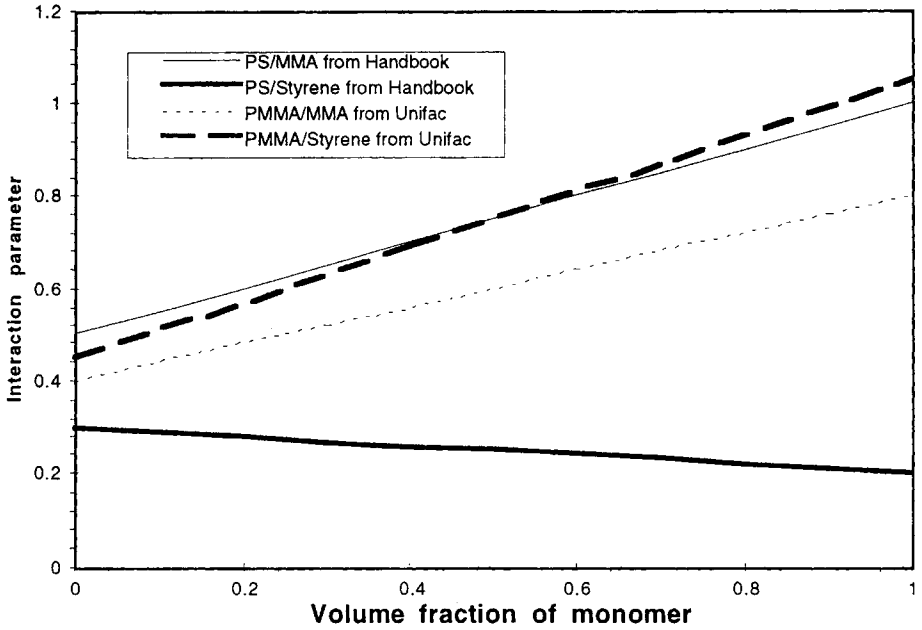

Figure 8 Interaction parameter between PS/MMA,[21] PS/styrene,[21] PMMA/MMA,[22] and PMMA/styrene[22] depending on polymer volume ratio.

inverted core–shell structure is predicted. The colors of the free-energy surface are alternated every 1 mN/m. At the bottom right of the figure are the values of the interfacial tensions (Gam1 = $\gamma_{P1/W}$, Gam2 = $\gamma_{P2/W}$, Gam12 = $\gamma_{P1/P2}$) calculated at the indicated conversion level. The conversion dependency of the particle morphology can be seen in the sequential outputs at 25, 50, 75, and 100% conversion for system I, as shown in Figures 10–13. As conversion increases, all the free energies increase (due to

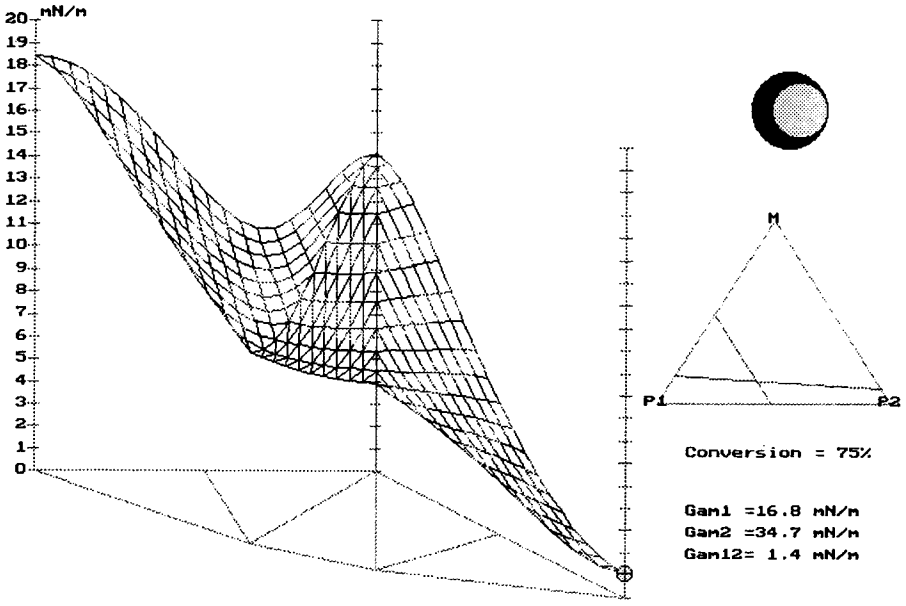

Figure 9 Graphic display of the morphology calculations for the PMMA/styrene/MXP system at 75% conversion.

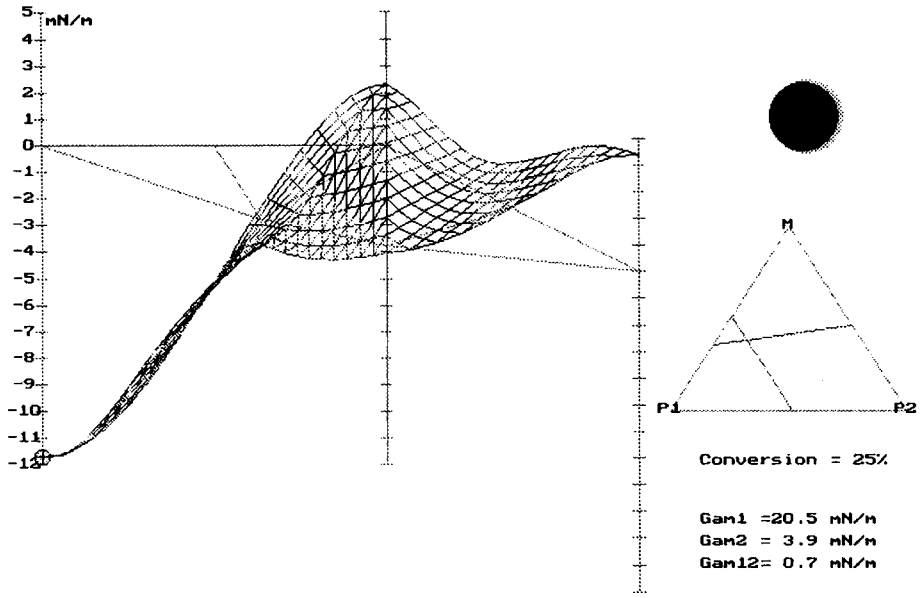

Figure 10 Graphic display of the morphology calculations for the PS/MMA/MXP system at 25% conversion.

increasing interfacial tensions with lower monomer concentrations) and the energy surface changes shape dramatically. However, for this system, the morphology always remains core–shell, with the PMMA accumulating at the aqueous interface. Winzor and Sundberg[12] also reported a core–shell morphology for this system.

In contrast to the results for system I, that of system II shows a rather hemispherical morphology at 75% monomer conversion, as seen in Figure 14. This is clearly due to dramatic changes in $\gamma_{P1/W}$ and $\gamma_{P2/W}$ brought about by the change in surfactants. The SDS lowers the aqueous/polymer phase interfacial tensions so greatly that there is not much dif-

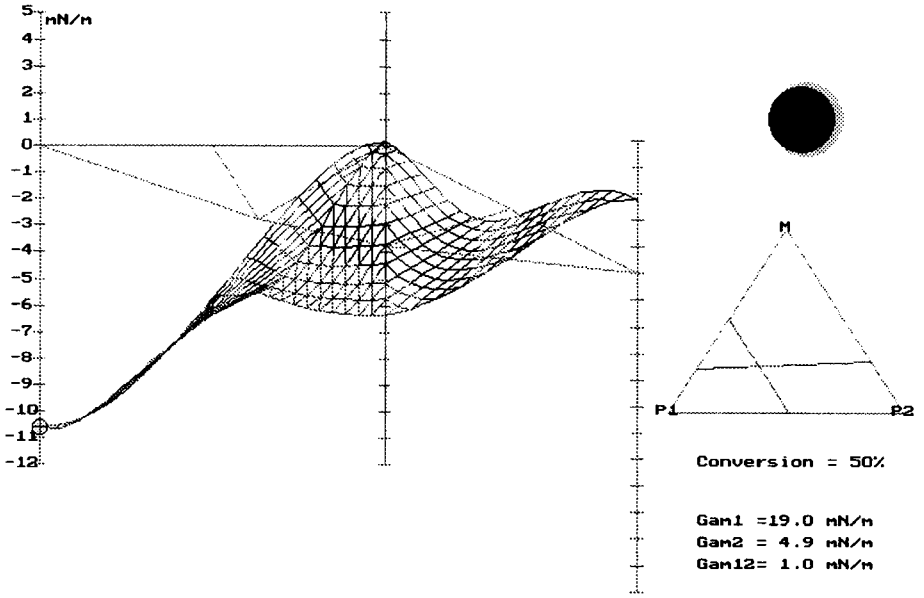

Figure 11 Graphic display of the morphology calculations for the PS/MMA/MXP system at 50% conversion.

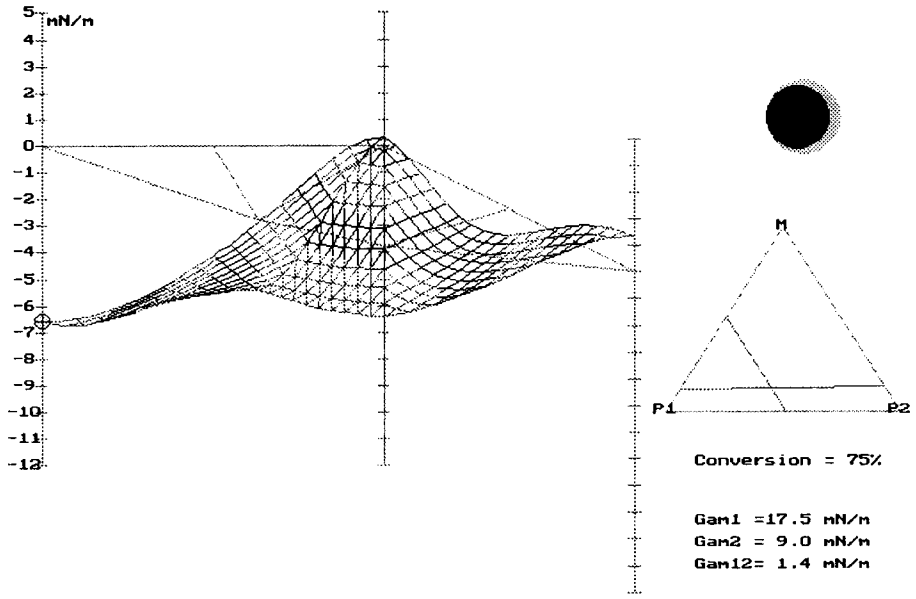

Figure 12 Graphic display of the morphology calculations for the PS/MMA/MXP system at 75% conversion.

ference between $\gamma_{P1/W}$ and $\gamma_{P2/W}$. This causes the internal interface between the two polymers to become an important contributor to the overall energy of the particle and the morphology shifts so as to minimize this interfacial area. These shifts in morphology are in agreement with the experimental results of Winzor and Sundberg.[12]

As indicated earlier, the above descriptions are limited to equilibrium conditions. However, we find that batch reaction conditions with relatively slow polymerization kinetics can yield experimental morphologies which are at or close to equilibrium conditions. Thus, one can readily study any of the parameters which may affect the various interfacial

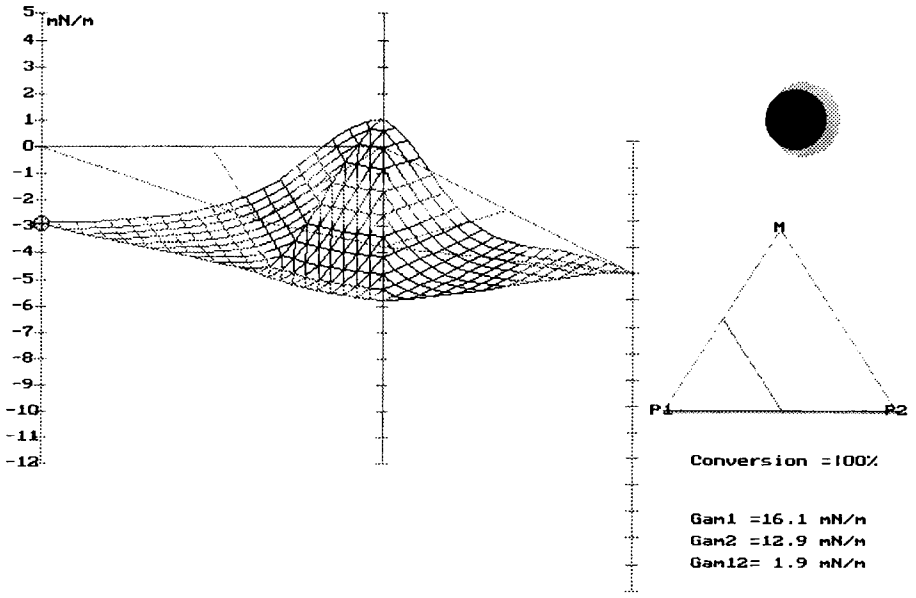

Figure 13 Graphic display of the morphology calculations for the PS/MMA/MXP system at 100% conversion.

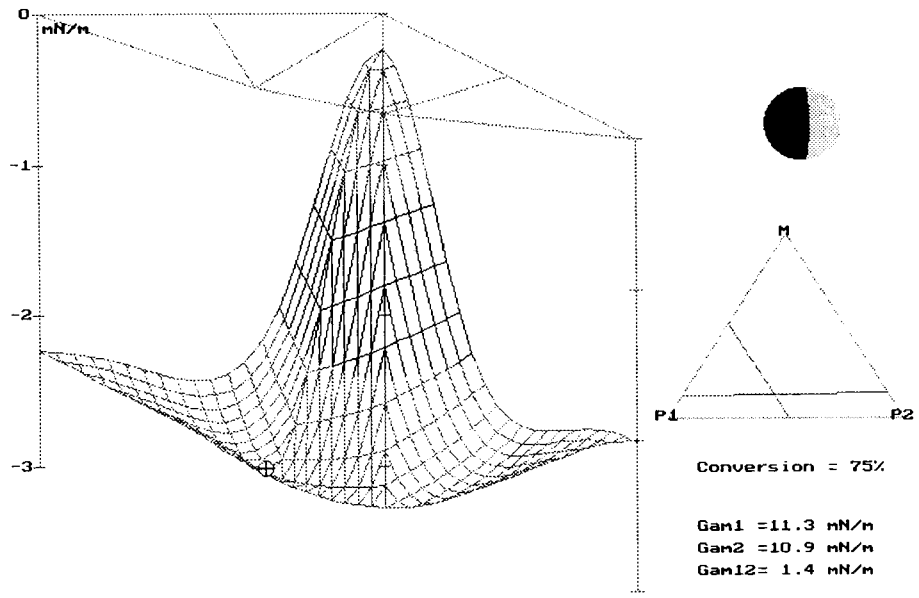

Figure 14 Graphic display of the morphology calculations for the PS/MMA/SDS system at 75% conversion.

tensions, such as surfactants, initiator end groups, comonomers, and the like.

CONCLUDING REMARKS

An interactive computer program is now available to predict conversion-dependent, equilibrium latex morphologies with a graphic display of the entire free-energy surface. On such a diagram, one cannot only identify the lowest point which corresponds to the preferred particle morphology, but also visualize the slope of the surface surrounding the minimum point. With steep contours adjacent to the minimum point, there is little doubt that the predicted morphology should match that found experimentally, assuming that the correct values of interfacial tensions have been used in the calculations. When the minimum point is located within a rather flat area on the energy surface, there are a variety of particles morphologies which possess nearly equal energies. In such a case, very accurate values of the interfacial tensions are required to obtain predictions in agreement with experiment. This constitutes a distinct advantage in our evolving understanding of the factors which control the equilibrium morphology of latex particles.

We are grateful for the partial financial support of Rhône-Poulenc and for the helpful mathematical discussions with Professor Claire Durant.

REFERENCES

1. I. Cho and K.-W. Lee, *J. Appl. Polym. Sci.*, **30,** 1903 (1985).
2. D. R. Stutman, A. Klein, M. S. El-Aasser, and J. W. Venderhoff, *Ind. Eng. Chem. Prod. Res. Dev.*, **23,** 404 (1985).
3. S. Lee and A. Rudin, *J. Polym. Sci. Part A Polym. Chem.*, **30,** 2211 (1992).
4. M. Okubo, M. Ando, A. Yamada, Y. Katsuda, and T. Matsumoto, *J. Polym. Sci. Polym. Lett. Ed.*, **19,** 143 (1981).
5. J.-E. Jönsson, H. Hassander, and B. Törnell, *Macromolecules,* **27,** 1932 (1994).
6. J. Berg, D. C. Sundberg, and B. Kronberg, *Polym. Mater. Sci. Eng.*, **54,** 367 (1986).
7. J. Berg, D. C. Sundberg, and B. Kronberg, *J. Microencapsul.*, **6,** 327 (1989).
8. D. C. Sundberg, A. J. Cassasa, J. Pantazopoulos, M. R. Muscato, B. Kronberg, and J. Berg, *J. Appl. Polym. Sci.*, **41,** 1425 (1990).
9. J.-E. Jönsson, H. Hassander, L. H. Jansson, and B. Törnell, *Macromolecules,* **24,** 126 (1991).
10. J. A. Waters, *Coll. Surf. A Physiochem. Eng. Ascp.*, **83,** 167 (1994).
11. Y. C. Chen, V. Dimonie, and M. S. El-AAsser, *Macromolecules,* **24,** 3779 (1991).
12. C. L. Winzor and D. C. Sundberg, *Polymer,* **18,** 3797 (1992).
13. C. L. Winzor and D. C. Sundberg, *Polymer,* **20,** 4269 (1992).
14. Y. G. Durant and J. Guillot, *Colloid Polym. Sci.*, **271,** 607 (1993).

15. E. J. Sundberg and D. C. Sundberg, *J. Appl. Polym. Sci.*, **47,** 1277 (1993).
16. Y. C. Chen, V. Dimonie, and M. S. El-AAsser, *J. Appl. Polym. Sci.*, **45,** 487 (1992).
17. S. Torza and S. G. Mason, *J. Coll. Int. Sci.*, **33,** 67 (1970).
18. I. Maxwell, J. Kurja, G. H. J. Van Doremaele, and A. L. German, *Makromol. Chem.*, **193,** 2049 (1992).
19. I. Maxwell, J. Kurja, G. H. J. Van Doremaele, and A. L. German, *Makromol. Chem.*, **193,** 2065 (1992).
20. Y. G. Durant, D. C. Sundberg, and J. Guillot, *J. Appl. Polym. Sci.*, **53,** 1469 (1994).
21. A. F. M. Barton, in *Handbook of Polymer-Liquid Interaction Parameters and Solubility Parameters,* CRC Press, Boca Raton, FL, 1990.
22. Y. G. Durant, D. C. Sundberg, and J. Guillot, *J. Appl. Polym. Sci.*, **52,** 1823 (1994).

Received February 16, 1995
Accepted April 23, 1995